AIChE

Hydrogenation of 2-Ethylanthraquinone Under Taylor Flow in Single Square Channel Monolith Reactors

Dingsheng Liu and Jianguo Zhang
Dalian Institute of Chemical Physics, Chinese Academy of Sciences, Dalian 116023, P.R. China
Graduate School of Chinese Academy of Sciences, Beijing 100039, P.R. China

Defu Li and Qingdan Kong
Dalian Institute of Chemical Physics, Chinese Academy of Sciences, Dalian 116023, P.R. China

Tong Zhang
Dalian Institute of Chemical Physics, Chinese Academy of Sciences, Dalian 116023, P.R. China
Graduate School of Chinese Academy of Sciences, Beijing 100039, P.R. China

Shudong Wang
Dalian Institute of Chemical Physics, Chinese Academy of Sciences, Dalian 116023, P.R. China

DOI 10.1002/aic.11696
Published online February 5, 2009 in Wiley InterScience (www.interscience.wiley.com).

The hydrogenation of 2-ethylanthraquinone (EAQ) to 2-ethylanthrahydroquinone (EAHQ) was carried out under Taylor flow in single square channel monolith reactors. The two opening ends of opaque reaction channel were connected with two circular transparent quartz-glass capillaries, where Taylor flow hydrodynamics parameters were measured and further used to obtain practical flow state of reactants in square reaction channels. A carefully designed gas-liquid inlet mixer was used to supply steady gas bubbles and liquid slugs with desired length. The effects of various operating parameters, involving superficial gas velocity, superficial liquid velocity, gas bubble length, liquid slug length, two-phase velocity and temperature, on EAQ conversion were systematically researched. Based on EAQ conversion, experimental overall volumetric mass transfer coefficients were calculated, and also studied as functions of various parameters as mentioned earlier. The film model, penetration model, and existing semi-empirical formula were used to predict gas-solid, gas-liquid, and liquid-solid volumetric mass transfer coefficients in Taylor flow, respectively. The predicted overall volumetric mass transfer coefficients agreed well with the experimental ones. © 2009 American Institute of Chemical Engineers *AIChE J,* 55: 726–736, 2009
Keywords: hydrogenation, conversion, mass transfer coefficient, Taylor flow, monolith reactor

Introduction

Multiphase monolith reactors are attracting more and more attention from laboratory to chemical industry, and considered as a very promising alternative to conventional gas-liq-

Correspondence concerning this article should be addressed to S. Wang at Wangsd@dicp.ac.cn.

uid-solid reactors.[1–6] In general, a monolith block consists of many straight, parallel, and uniform channels with square, circle, triangle or other geometric cross sections, which have typically 1–5 mm hydraulic diameters. The structures make monolith reactors possess several advantages: low pressure drop, high mass transfer rate, ease of scale-up and so on.[1–6] Monolith reactors can be used to economically intensify gas-liquid-solid mass transfer, and further enhance the yield and selectivity for competitive series/parallel reactions. One worthy notice is that monolith reactor performances are seriously affected by multiphase flow patterns existed in the channels.[7–9] At different superficial gas and liquid velocities, different flow patterns are observed. One two-phase flow pattern called Taylor flow is easily obtained in the wide range of superficial gas and liquid velocities, and has superior mass transfer characteristics. Taylor flow consists of trains of long bubbles separated by liquid slugs. The gas-to-wall mass transfer is increased remarkably because of the existence of thin liquid films between bubbles and channel walls. Recirculation velocity fields are induced in liquid slugs trapped between two consecutive bubbles, which enhances the radial mass transfer greatly, and makes concentration of solute more uniformly. The axial segregation of bulk liquid reduces the axial dispersion of solute, and makes the liquid phase residence time distribution narrower.[10–12]

During the past two decades, mass transfer and reaction under Taylor flow in monolith and microchannel reactors were researched. Bercic and Pintar[13] measured the gas-liquid and liquid-solid mass transfer in circular capillaries. They presented two simple correlations used to predict mass transfer coefficient, which showed that mass transport were mostly determined by liquid slug lengths, gas bubble lengths and two-phase velocities.[13] By means of computational fluid dynamics (CFD), Baten and Krishna investigated mass transfer from gas phase to liquid phase and from solid phase to liquid phase in circular capillaries.[14,15] Their results showed that penetration theory could be used to calculate gas-liquid mass transfer coefficient for short contact time between bubbles and liquid films.[14] As for liquid-solid mass transfer, they fitted an empirical correlation for practical estimation of mass transfer coefficient based on Taylor flow hydrodynamics.[15] Vandu and Krishna obtained gas-liquid mass transfer coefficient under Taylor flow from experimental oxygen absorption dynamics.[16] The experimental values were in good agreement with the model developed by Baten and Krishna,[14] with the additional assumption that the dominant mass transfer contribution is to the liquid film.[16] Bercic checked the influences of the operating conditions on observed reaction rates in single circular channel reactors operated in Taylor flow regime by investigating catalytic hydrogenation of nitrobenzoic acid (NBA) to aminobenzoic acid.[17] The result showed that at high concentrations of NBA, the reaction was controlled by the hydrogen mass transport while at low concentration the mass transport of NBA was dominant.[17] The same reaction was also studied under vertical two-phase flow in a circular capillary by Tsoligkas and Simmons.[7] They considered that, compared with other flow patterns, Taylor flow was the optimum with the reaction rate dependent on the liquid slug length.[7] Natividad et al.[18] and Tsoligkas et al.[19] studied the hydrogenation of 2-butyne-1,4-diol on Pd catalyst under Taylor flow in monolith and capillary reactors. Their experiments showed that the operating condition of Taylor flow influenced remarkably the initial reaction rate.[18,19]

It was well known that, compared with circular channels, square channel monolith reactors were more widely used in practice. The flow states of reactants in square channels were remarkably different from that in circular channels. Though many reactions were tested in square channel monolith reactors, the relationship between reactions and Taylor flow operating parameters, for example liquid slug length and gas bubble length, were not studied carefully until now. As monolith reactors were opaque, flow states existed in the channels were not observed directly. Though Magnetic resonance, capacitance tomography etc. have been successfully used to characterize visually gas-liquid flow in monolith channels,[20,21] these techniques were expensive, complicated and inconvenient. In addition, because of the limitation of experiment set-ups, various operating parameters were not changed independently in some reports, which resulted that only effects of limited parameters on mass transfer and reaction were considered.

The main objective of this work was to understand the characteristics of multiphase reactions under Taylor flow in square channel monolith reactors. The effects of various operating parameters on reaction conversions and overall volumetric mass transfer coefficients were checked systematically. Circular transparent quartz-glass capillaries were connected with the opening ends of square reaction channels to study visually Taylor flow. Hydrodynamics parameters measured in transparent capillaries, together with a reasonable geometry model proposed here, were used to get various Taylor flow parameters in reaction channels. A carefully designed gas-liquid inlet mixer was used to supply steady gas bubbles and liquid slugs with desired lengths. Here, catalytic hydrogenation of 2-ethylanthraquinone (EAQ) to 2-ethylanthrahydroquinone (EAHQ) over Pd/Al_2O_3 was adopted as a model reaction. The reaction was one important step of production of hydrogen peroxide via anthraquinone process. The hydrogenation product (EAHQ) was further oxidized with oxygen (or air), and resulted in hydrogen peroxide and the regeneration of EAQ. The completely cyclic reaction route was depicted in Figure 1.

Experimental

Chemicals

The solid EAQ was dissolved in an organic solvent consisting of trioctyl phosphate and trimethylbenzene. The volume ratio of trioctyl phosphate to trimethylbenzene was 1:3. The concentration of EAQ employed in the solution was a constant value: 0.396 mol/L. Pure hydrogen was used as a gas reactant. The viscosity of EAQ solution was measured using rotation viscosity meter. The diffusivity and solubility of hydrogen in EAQ solution and the surface tension of EAQ solution were estimated based on the methods in Refs. 22 and 23 and were listed in Table 1.

The preparation of single channel monolithic reactors

Bare cordierite monolithic modules, consisting of nine 1×1 mm^2 channels with 200 mm length, were adopted as

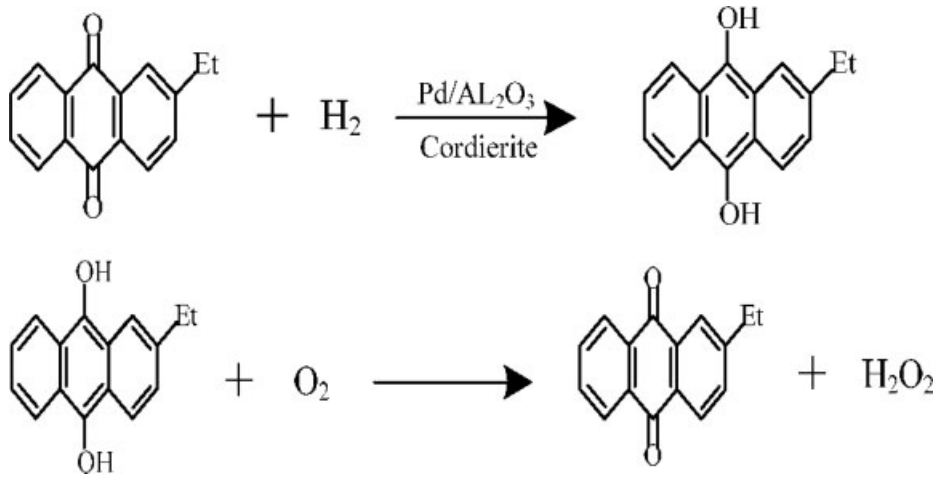

Figure 1. The reaction route of production of hydrogen peroxide via anthraquinone process.

catalyst supports. The monolithic supports were firstly washcoated with a layer of γ-alumina, which increased dramatically the specific surface of supports. Then dried washcoated monoliths were further dipped into $PdCl_2$ solution (99.10 mg/mL) to load active component Pd. Finally, the monolith catalyst containing 4.5% by weight Pd was prepared. In the process of catalyst preparation, special care must be given to obtain uniform active metal deposition on the walls in both radial and axial directions. The similar post-process method to Wei[24] was adopted to turn further monolith catalysts into single channel reactors. As shown in Figure 2, except for the center channel, the other eight channels were filled with fine SiO_2 powders and sealed with inert heat-resistant gluewater at the top and bottom openings. The peripheries of monolith modules were also coated with the gluewater to prevent possible leakage. The two openings of isolated central channel were connected to transparent circular quartz-glass capillaries with nearly equal hydraulic diameter to the central square channel. The precise internal diameters were determined by imaging the capillary cross-sections using a microscope. The lengths of inlet and outlet circular capillaries were 0.3 m. In order to control conveniently the reaction temperature, the prepared single channel reactors, together with temperature transducers, were sealed in quartz-glass water bath tubes. Then, the whole module containing a single channel reactor was fixed in the U-box of experimental set-up (see Figure 3) to carry out hydrogenation of EAQ.

Table 1. Physical Properties of EAQ Solution and Hydrogen

	EAQ Solution		Hydrogen	
Temperature (°C)	Viscosity (mPa · S)	Surface Tension (m*N*/m)	Diffusivity in EAQ Solution (m^2/s)	Solubility in EAQ Solution (0.4 MPa) (mol/mL)
20	1.07	31.83	5.03E-9	1.12E-5
30	0.98	30.74	5.62E-9	1.23E-5
40	0.97	29.64	5.91E-9	1.29E-5
50	0.89	28.54	6.75E-9	1.35E-5
60	0.87	27.44	7.07E-9	1.39E-5
70	0.84	26.34	7.56E-9	1.46E-5
80	0.80	25.25	8.34E-9	1.50E-5

Experimental setup and procedure

The experimental setup of hydrogenation reaction in a single channel monolith reactor was illustrated clearly in Figure 3. To force EAQ solution through the reactor at a smoothly constant velocity, a tank with invariable pressure was designed to supply the solution. The solution velocity was controlled by a liquid rotameter between the tank and mixer. The hydrogen velocity was adjusted by a mass flow meter.

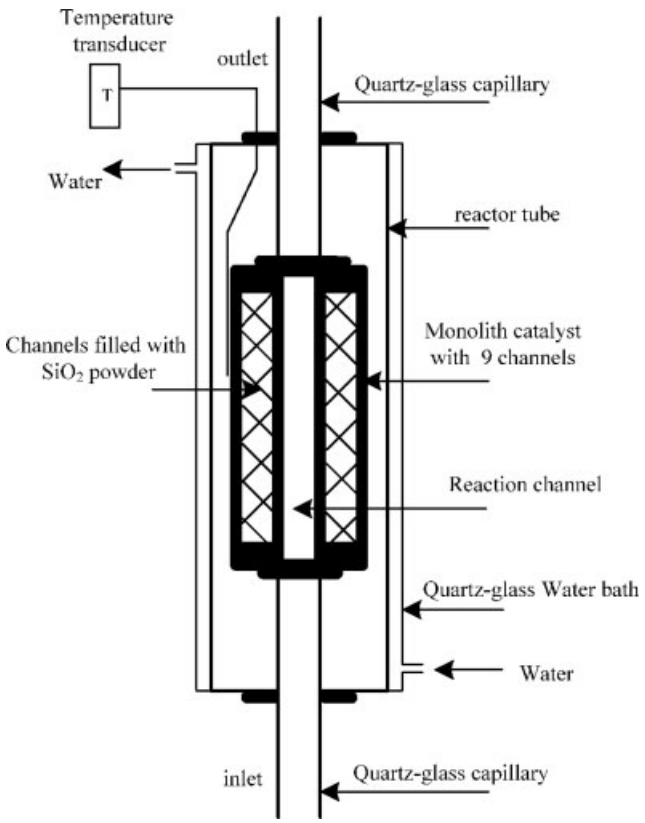

Figure 2. A single square channel monolith reactor in a quartz-glass water bath.

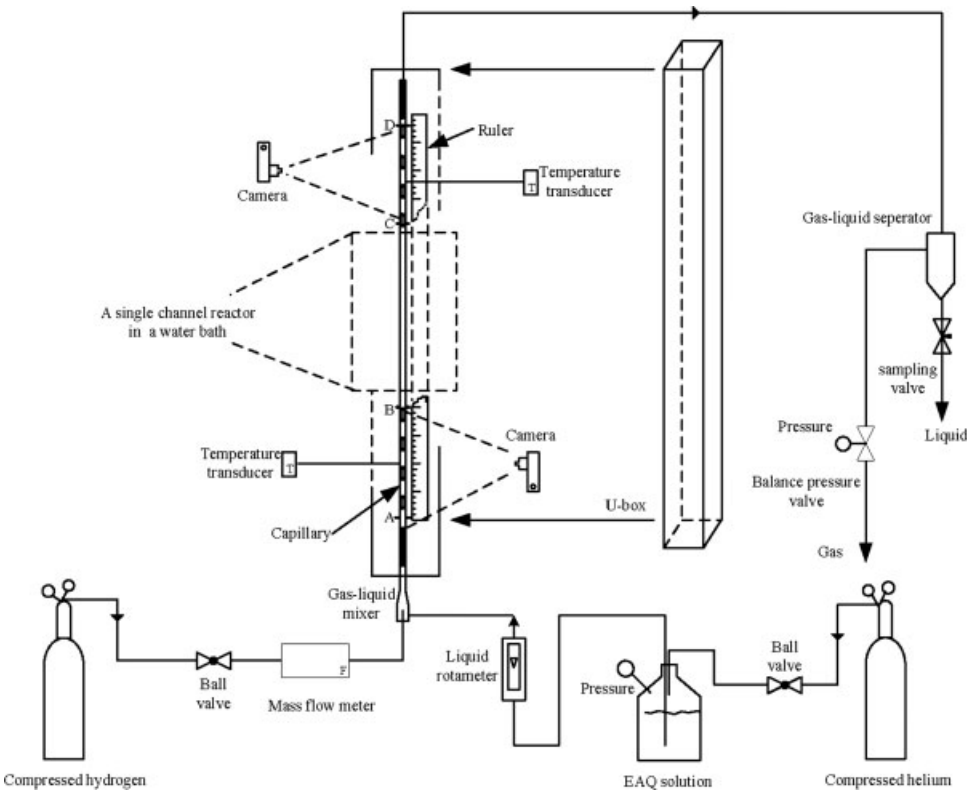

Figure 3. Schematic diagram of experimental setup.

Figure 3 showed that the EAQ solution and hydrogen were fed into the reactor from the side and bottom of the gas-liquid mixer, respectively. The detailed structure of mixer was depicted in Figure 4, which was similar to that used by Kreutzer et al.[25] Generally, the bubble size was determined by the gas orifice diameter. In order to obtain gas bubbles with different lengths, various delivery gas channels with different orifice diameters were adopted. In Figure 3, the distances from point A to B and from C to D were known in advance, through which the time taken by the bubbles traveled was measured using a stopwatch. Thus, the bubble velocities in circular capillaries were obtained, which were further used to determine the corresponding actual bubble velocities in square reaction channels. The flow patterns before and after single channel reactors were captured by a digital charge-coupled device (CCD) camera with the shutter speed of 1/1000 s, and then were saved into a hard driver of personal computer for later analysis. Rulers (Plotting papers) were pasted on the U-box wall behind the capillaries to estimate roughly the bubble and slug lengths; and the accurate lengths were carefully determined from the digital photos using more precision digital scales. From Figure 2, the reactants flowed from the inlet circular capillary to the square reaction channel, and again to the outlet circular capillary. By comparing the flow patterns and the number of Taylor bubbles per unit time passed the mark places in the inlet and outlet capillaries, flow states in square channel can be judged as steady or not. During the experiment, operating conditions were carefully controlled in order to avoid the coalescence and split of Taylor bubbles resulted from the change of channel geometries. The hydrogenation solution was analyzed by Agilent-6890-GC-5973-MS, and no by-products were observed under the experimental conditions. The fluids temperature in

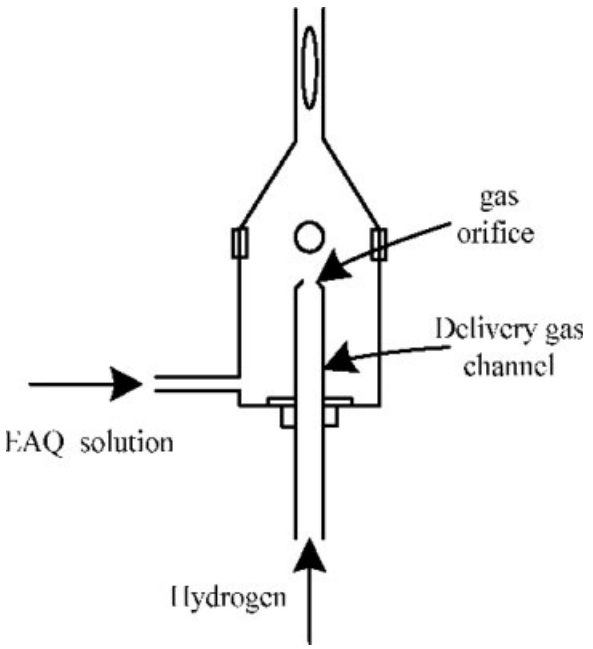

Figure 4. Gas-liquid mixer.

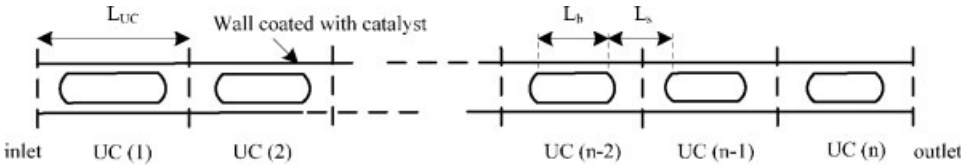

Figure 5. Taylor flow with chemical reaction in a channel.

capillaries was measured using temperature transducers. The reaction pressure was a constant value, 0.4 Mpa.

Analytical method

The hydrogenation solution sampled at the exit of gas-liquid separator was diluted with de-ionized water, and then oxidized with flowing air. Hydrogen peroxide was obtained as an oxidization product, and EAHQ was reduced to EAQ. Hydrogen peroxide in the oxidization mixer was extracted with de-ionized water. In the presence of sulfuric acid, the extraction products were titrated with standard potassium permanganate solution in order to determine the amount of hydrogen peroxide. Based on the stoichiometric ratio of the reaction in Figure 1, the amount of EAQ consumed was calculated from the amount of hydrogen oxide. EAQ conversion, X, was defined as follows:

$$X = (C_{\mathrm{EAQ}}^{\mathrm{in}} - C_{\mathrm{EAQ}}^{\mathrm{out}})/C_{\mathrm{EAQ}}^{\mathrm{in}} \tag{1}$$

Theoretical Consideration

Geometry model

Figure 5 showed that hydrogen and EAQ solution flowed under Taylor flow in a reaction channel coated with catalyst. Here, one combination of a Taylor bubble and two close half-liquid-slugs was called a "unit cell." With flowing, the hydrogenation of EAQ proceeded on the catalyst wall, and hydrogen consumed gradually along the reaction channel. The Taylor bubble at the channel outlet was remarkably shorter than that at the channel inlet. At the same time, the moving velocities of bubbles also decreased along the flow direction because of the decrease of gas reactant volume. With bubbles consuming, the original liquid, accumulated around the bubbles, mixed into the neighboring liquid slugs, so the liquid slug at the channel outlet became longer despite the change was very slight. In this work, catalyst layer coated on channel walls was very thin and its influence on the geometry of square channels was negligible. Different from that in circular channels, Taylor bubbles in square channels were not circular symmetric at low and medium capillary numbers, i.e., Ca < 0.1, and flatted out against the walls leaving accumulative liquids in the corners[9,26,27] as shown in Figure 6. The film thickness was not uniform around the bubble. Kolb and Cerro[26] and Thulasidas et al.[27] measured experimentally bubble radius at different Ca in AB and AC directions in Figure 6. In general, at Ca < 0.04, the bubble radius in AB direction (R_{side}) was virtually independent of Ca, and $R_{\mathrm{side}}/R_{\mathrm{c}}$ was a nearly constant value, 0.95.[26] The bubble radius in AC direction ($R_{\mathrm{diag.}}$) could be determined approximately as follows[1,5]:

$$R_{\mathrm{diag.}}/R_{\mathrm{c}} = 0.7 + 0.5\exp(-2.25Ca^{0.445}) \tag{2}$$

In this work, $0.0003 <$ Ca < 0.002 were covered, under which the variation of $R_{\mathrm{diag.}}$ was very slight, and $R_{\mathrm{diag.}}$ was assumed as a constant value. For simplicity, $R_{\mathrm{diag.}}/R_{\mathrm{c}} = 1.2$ was adopted in the whole range of Ca. The function relations between various geometric parameters, describing cross sections of Taylor bubbles in square channels in Figure 6, were established according to the rules given in the appendix B of Kolb and Cerro's paper.[26] As mentioned previously, Taylor flow patterns in transparent quartz-glass capillaries were captured by a CCD camera, and used to deduce the actual Taylor flow patterns in square reaction channels. For simplicity, the cap of Taylor bubble was assumed as hemi-sphere with a radius approximately equaled to channel hydraulic radius in both quartz-glass capillaries and square reaction channels. In general, the fluid temperature in quartz-glass capillaries was different from that in reaction channels. Here, it was assumed that liquid density was constant, while gas was perfect. By means of perfect gas state equation, gas bubble volumes in reaction channel inlets and outlets were obtained from that in transparent capillaries. Thulasidas et al.[27] showed that the gas bubble and liquid slug velocities were related by

$$A_{\mathrm{b}}V_{\mathrm{b}} = A_{\mathrm{c}}U_{\mathrm{s}} + Q_{\mathrm{film}} \tag{3}$$

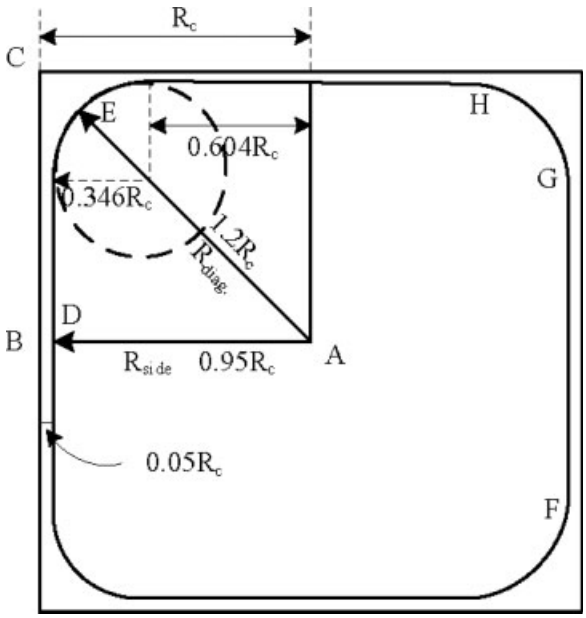

Figure 6. Geometry variables of the cross section of Taylor bubble.

where Q_{film} was liquid film volumetric flow rate surrounding bubbles. In this work, the contact time between bubbles and liquid films was short, which resulted that the flow of liquid did not develop fully. For simplicity, Q_{film} was assumed as zero, i.e., $Q_{film} = 0$.

Mass transfer model

Under Taylor flow in square channels, four different mass transfer stages for hydrogen transport to the catalyst wall were identified: (1) hydrogen transfers from bubbles, through the flat liquid films between surface GF (see Figure 6) and channel walls, directly to the catalyst wall, (GS), (2) hydrogen transfers from bubbles through arc surface HG (see Figure 6) to the liquids accumulated in the corners of square channel, (GL_corner); (3) hydrogen transfers from the caps of bubbles to liquid slugs, (*GL_cap*), (4) the transfer of dissolved hydrogen from liquid slugs and liquids accumulated in the corners of square channel to the catalyst wall (*LS*). In the simplest approximation, all possible overlap and interaction between these transfer steps were ignored. The gas-liquid and liquid-solid mass transfer was considered as resistance in series and were in parallel with respect to the gas-solid mass transfer. Thus, the overall volumetric mass transfer coefficient could be expressed as follows:

$$K\alpha = K_{GS}\alpha_{GS} + \left(\frac{1}{K_{GL\_corner}\alpha_{GL\_corner} + K_{GL\_cap}\alpha_{GL\_cap}} + \frac{1}{K_{LS}\alpha_{LS}}\right)^{-1} \quad (4)$$

The flat liquid film, through which gas-solid mass transfer proceeded, was very thin and the liquid velocity in the film was negligible. The film model could be used to evaluate gas-solid mass transfer coefficient[5]:

$$K_{GS} = \frac{D}{\delta} \quad (5)$$

$$\alpha_{GS} = \frac{2.416L_b}{d_c(L_b + L_s)} \quad (6)$$

The liquid film between arc surface HG and channel wall was not uniform, and was very thick. In the two different regions, gas-liquid mass transfer coefficients were all calculated by means of the penetration theory[14,28] and written as:

$$K_{GL\_corner} = 2\sqrt{\frac{DV_b}{\pi L_b}}, \quad (7)$$

$$\alpha_{GL\_corner} = \frac{0.346\pi L_b}{(L_b + L_s)d_c}, \quad (8)$$

$$K_{GL\_cap} = 2\frac{\sqrt{2}}{\pi}\sqrt{\frac{DV_b}{d_c}}, \quad (9)$$

$$\alpha_{GL\_cap} = \frac{\pi}{(L_b + L_s)}. \quad (10)$$

The existing reports about liquid-solid mass transfer in square channels were rare. Baten and Krishna studied numerically liquid-solid mass transfer in circular capillaries and presented a set of formulas to evaluate liquid-solid mass transfer coefficient, which was used to estimate roughly that in square channels.[15] The formulas were listed as follows:

$$\frac{K_{LS}d_c}{D} = \frac{\beta}{Gz_c^{\xi}}, \quad (11)$$

Where

$$\zeta = 0.61Gz_s^{0.025}, \quad (12)$$

$$\beta = \frac{0.5}{(Gz_s/\varepsilon_G)^{0.15}}, \quad (13)$$

$$Gz_s = \frac{L_s D}{d_c^2 V_b}, \quad (14)$$

$$Gz_c = \frac{L_c(1-\varepsilon_G)D}{d_c^2 V_b}. \quad (15)$$

The specific surface of liquid-solid mass transfer was

$$\alpha_{LS} = \frac{4L_s + 1.584L_b}{(L_b + L_s)d_c} \quad (16)$$

At steady state, the overall hydrogen transfer rate from bubbles to catalysts was the same to the reaction rate, then

$$r_{obs} = K\alpha(C^*_{H_2} - C^{wall}_{H_2}) \quad (17)$$

Hydrogenation of EAQ over Pd catalyst was a very fast reaction, and mass transfer played an important role in determining the reaction rate.[29,30] The concentration of hydrogen on the catalyst wall was much lower than the equilibrium concentration, and approximately equaled to zero, i.e. $C^{wall}_{H_2} \approx 0$. The equilibrium concentration of hydrogen in EAQ solution was listed in Tab. 1. Based on the definition of reaction rate and stoichiometric ratio in Figure 1, the present reaction rate was also expressed as

$$r_{obs} = \frac{C^{in}_{EAQ}X}{L_c/U_{TP}} \quad (18)$$

Substituted Eq.18 into Eq. 17, then

$$K\alpha = \frac{C^{in}_{EAQ}XU_{TP}}{C^*_{H_2}L_c}. \quad (19)$$

Results and Discussion

Effect of various operating parameters on EAQ conversion

Figures 7–12 illustrated the effect of various operating parameters on EAQ conversion in single channle monolith reactors operated under Taylor flow regime. Taylor flow parameters varied along reaction channels with reactants flowing, and the values of parameters given in Figures 7–12,

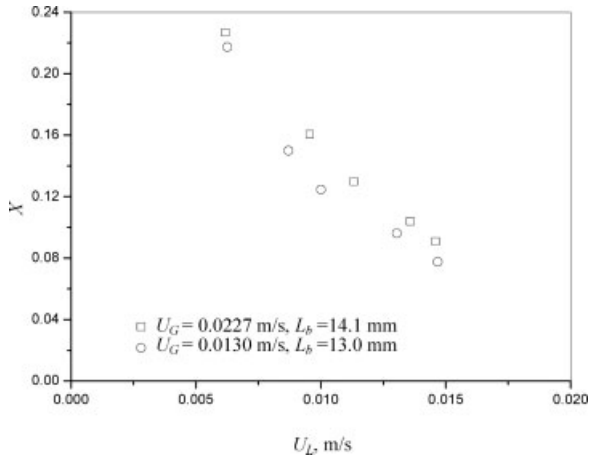

Figure 7. Effect of superficial liquid velocity on EAQ conversion.

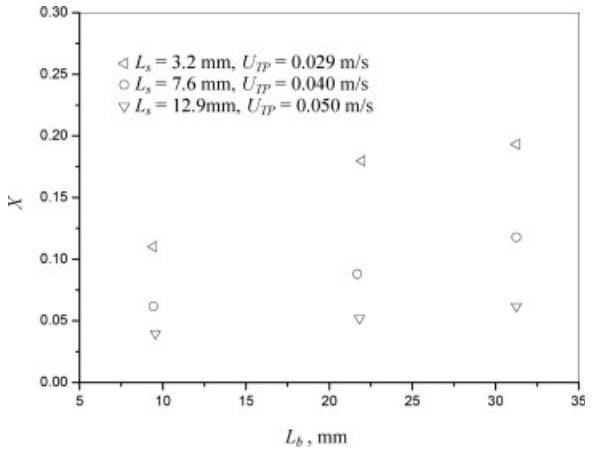

Figure 9. Effect of bubble length on EAQ conversion.

except for EAQ conversion, were all evaluated at reaction channel inlets. EAQ conversion was calculated from whole reaction channels by means of Eq. 1.

Figure 7 showed that EAQ conversion decreased remarkably with increasing superficial liquid velocities at constant U_G and L_b. While, in Figure 8, the conversion increased slowly with increasing superficial gas velocities at fixed U_L and L_b, though the effect of U_G on the conversion was slight. It was known that reaction channel walls, where the hydrogenation reaction proceeded, could be divided into two regions: one region around Taylor bubbles, called bubble wall region and the other region around liquid slugs, called slug wall region. The increase of U_L in Figure 7 resulted that bubble wall regions decreased, and slug wall regions increased in whole reaction channels. On the contrary, the increase of U_G in Figure 8 made that slug wall regions became smaller, and bubble wall regions became larger. Increase of U_L or U_G brought faster two-phase velocity, U_{TP} in Figures 7 and 8. Whereas, different from Figure 7, faster U_{TP} did not reduce EAQ conversion in Figure 8. Considered systematically the change trends of conversion in Figures 7 and 8, one conclusion was presented: the hydrogenation of EAQ mainly occured on bubble wall region, and the contribution from slug wall region to the reaction was minor. That meant that EAQ conversion increased with the ratio L_b/L_s increasing and the bubble velocity V_b decreasing. In Figure 7, with U_L increasing, the ratio L_b/L_s decreased and V_b increased, which together resulted that the conversion decreased. In Figure 8, with U_G increasing, both L_b/L_s and V_b increased. The effects of L_b/L_s and V_b on the conversion was opposite, which resulted that the overall effect of U_G on the conversion was slight in Figure 8.

At constant two-phase velocities, Figures 9 and 10 showed that EAQ conversion increased with lengthening gas bubbles at fixed liquid slug lengths, and decreased with enhancing slug lengths at fixed bubble lengths, respectively. It was worthy to note that two-phase velocity, U_{TP}, might be considered to be approximately equal to bubble velocity, V_b, which was also confirmed in the experiment. Figure 11 illustrated that the conversion increased with L_b/L_s increasing at a constant U_{TP}, and decreased with U_{TP} increasing at a fixed L_b/L_s. The change tends of EAQ conversion in Figures 9–11 all supported the conclusions drawn in Figures 7 and 8: EAQ conversion increased with bubble wall regions increasing, while decreased with bubble velocity increasing.

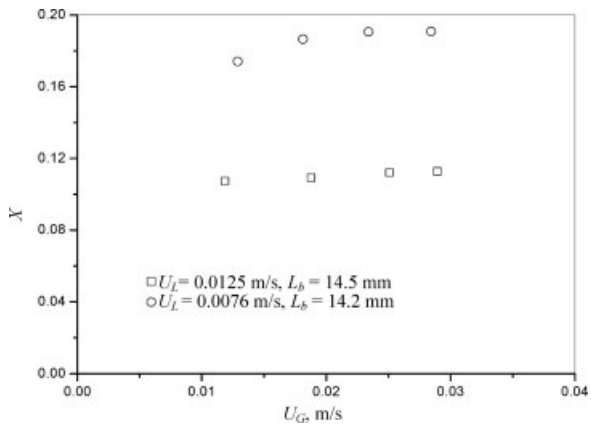

Figure 8. Effect of superficial gas velocity on EAQ conversion.

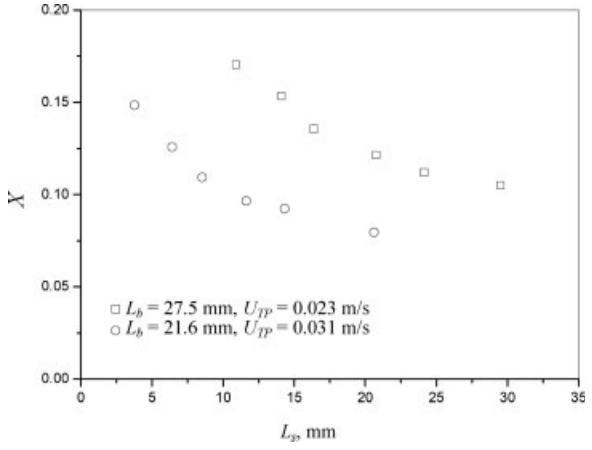

Figure 10. Effect of liquid slug length on EAQ conversion.

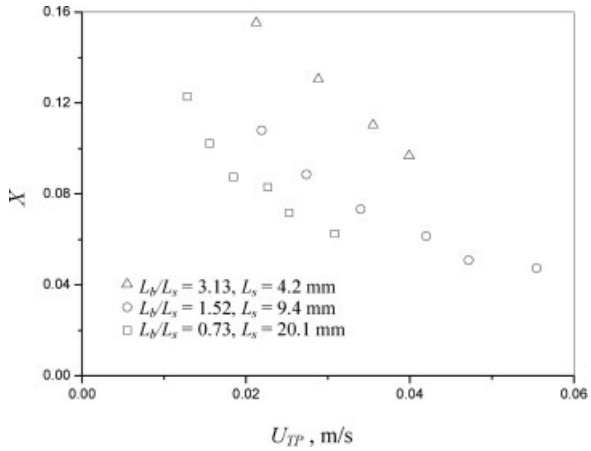

Figure 11. Effect of two-phase velocity on EAQ conversion.

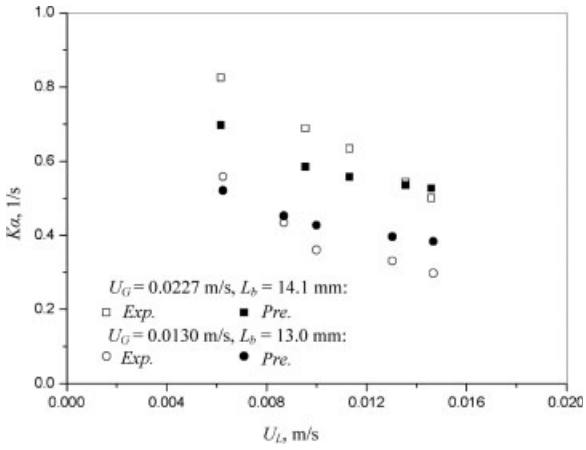

Figure 13. Effect of superficial liquid velocity on overall volumetric mass transfer coefficient.

Figure 12 showed conversion vs. temperature data at constant superficial gas and liquid velocities. Noted that superficial gas and liquid velocities labeled in Figure 12 were equivalent values at 20°C, transformed from inlet values in reaction channel at practical operation temperature, which was helpful to show the dependence of EAQ conversion on temperature at a same criterion. The effect of temperature on the conversion mainly ascribed to two causes: (1) the intrinsic reaction rate became faster with increasing temperature; (2) the bubble volume expanded and two-phase velocities increased at higher temperature. Because the hydrogenation of EAQ over Pd catalyst was a very fast reaction and restricted by mass transfer as previously discussed in *mass transfer model*, the first cause mentioned earlier was eliminated. The expansion of gas bubbles made the ratio L_b/L_s and U_{TP} increased. From Figure 11, the effects of the ratio L_b/L_s and U_{TP} on the conversion were opposite. In Figure 12, the overall results showed that the conversion increased with temperature increasing, which indicated that, compared with U_{TP}, the effect of L_b/L_s on the conversion was more important. From Figure 12, two-phase velocities at the channel inlets were nearly equal under two series of operation conditions. Therefore, Figure 12 also showed that, at constant inlet two-phase velocities and reaction temperatures, the conversion was larger at a higher ratio U_G/U_L, which was approximately equivalent to L_b/L_s.

Effect of various operating parameters on volumetric mass transfer coefficient

Based on Eq. 19, the experimental overall volumetric mass transfer coefficient, $(K\alpha)_{Exp.}$, was calculated from EAQ conversion. The effect of predissolved hydrogen, in EAQ solution through inlet circular capillaries, on $(K\alpha)_{Exp.}$ was negligible for the amount of predissolved hydrogen was very small, which was verified by the plug-flow model and empirical formula proposed by Bercic and Pintar.[13] By means of the geometry and mass transfer models presented in theoretical consideration, predicted overall volumetric mass transfer coefficient, $(K\alpha)_{Pre.}$, was obtained. Figures 13–18 showed the dependence of $K\alpha$ on various operating parameters under the same conditions to that given in Figures 7–12, respectively. Here, $K\alpha$ was evaluated from the whole reaction channels. During calculating $K\alpha$, the values of flow parameters in

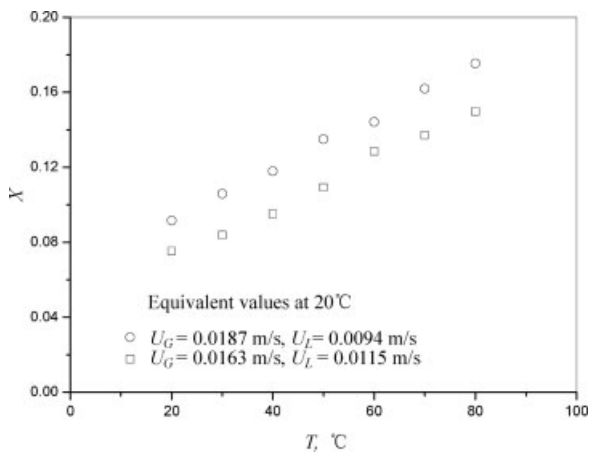

Figure 12. Effect of temperature on EAQ conversion.

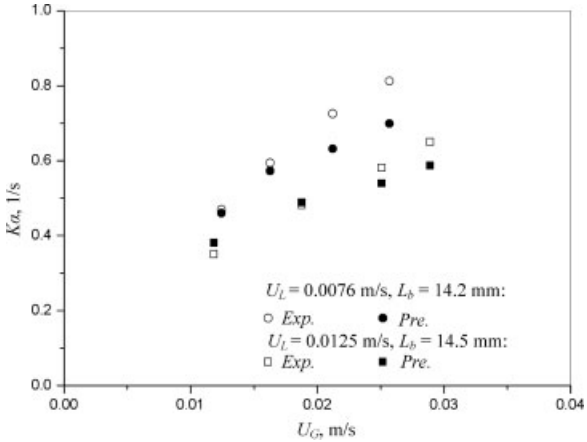

Figure 14. Effect of superficial gas velocity on overall volumetric mass transfer coefficient.

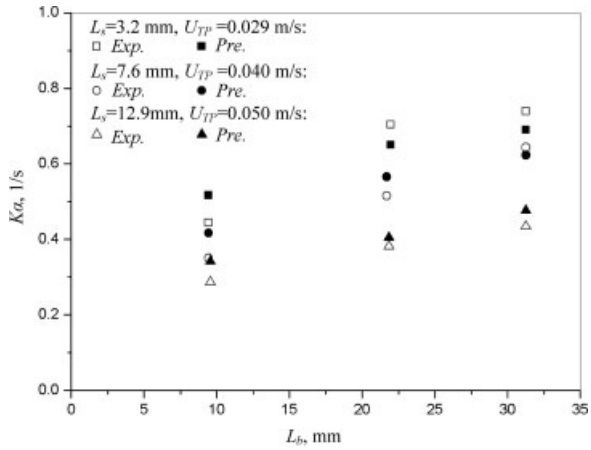

Figure 15. Effect of bubble length on overall volumetric mass transfer coefficient.

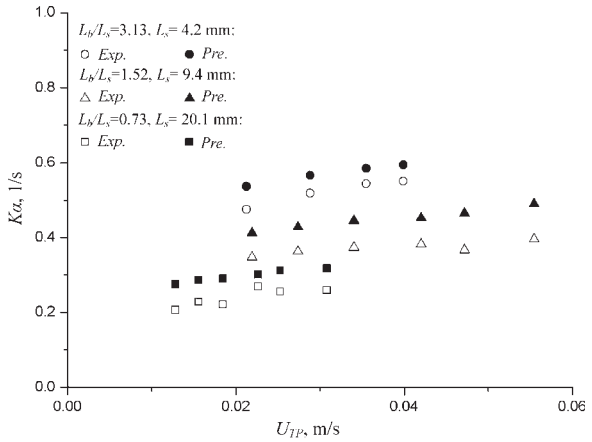

Figure 17. Effect of two-phase velocity on overall volumetric mass transfer coefficient.

Eqs. 5–19, except special designated parameters, were logarithmic mean of reaction channel inlet and outlet values. Because of the complicated formations of Eqs. 11–15, the relationship between K_{LS} and operating parameters was unapparent. Fortunately, Baten and Krishna[15] indicated that K_{LS} decreased with increasing channel Graetz number, Gz_c, which was also confirmed in our work. It was relative easy to analyze the effects of operating parameters on Gz_c in Eq. 15. Here, C_{EAQ}^{in} and L_c were constant, and $C_{H_2}^*$ was a function of reaction temperature. Eq. 19 showed that Ka was direct proportion to the conversion per unit time. Therefore, the change trends of experimental overall volumetric mass transfer coefficient vs. operating parameters in Figures 13–18 could be qualitatively judged from Figures 7–12, respectively.

Figure 13 showed the effect of superficial liquid velocities on overall volumetric mass transfer coefficient. Increases of U_L resulted in longer liquid slugs, faster bubble velocities and larger liquid holdup, which influenced four different stages volumetric mass transfer coefficients. In Eqs. 5–16, when liquid slugs was longer, the specific areas α_{GS}, α_{GL_corner} and α_{GL_cap} were smaller, but α_{LS} was larger. Faster bubble velocities resulted in larger K_{GL_corner} and K_{GL_cap}. K_{GS} was not influenced by superficial liquid velocities. The effects of liquid holdup $(1-\varepsilon_G)$ and bubble velocity V_b on Gz_c were opposite. The calculation showed that the change of K_{LS} was slight under the conditions in Figure 13. The overall results showed that $(K\alpha)_{Pre.}$ decreased with increasing U_L, which was similar to the change trend of $(K\alpha)_{Exp.}$. Figure 14 demonstrated that $K\alpha$ increased with superficial gas velocities increasing. At fixed U_L and L_b, increases of U_G resulted in shorter liquid slugs, faster gas bubble velocity and larger gas holdup, from which the change trends of different stages volumetric mass transfer coefficients were obtained in Eqs. 5–16. It was evident that the influence of U_G on the volumetric mass transfer coefficients was larger than on the reaction conversions in Figure 8. Figures 15 and 16 showed plots of volumetric mass transfer coefficients to gas bubble lengths and liquid slug lengths, respectively. Similar to Figures 9 and 10, $K\alpha$ increased with lengthening gas bubbles, and decreased with increasing liquid slugs. The effects of gas bubble length and liquid slug length on volumetric mass transfer coefficient were also revealed in mass transfer models (see Eqs. 5–16). Figure 17 illustrated a

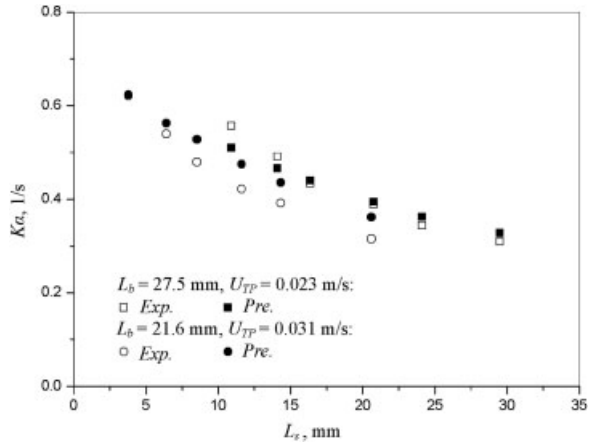

Figure 16. Effect of liquid slug length on overall volumetric mass transfer coefficient.

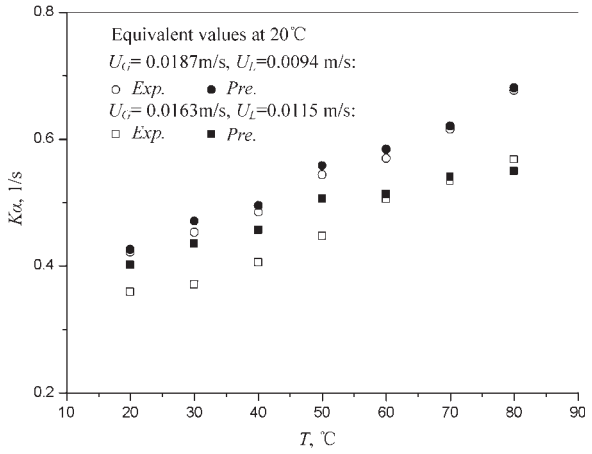

Figure 18. Effect of temperature on overall volumetric mass transfer coefficient.

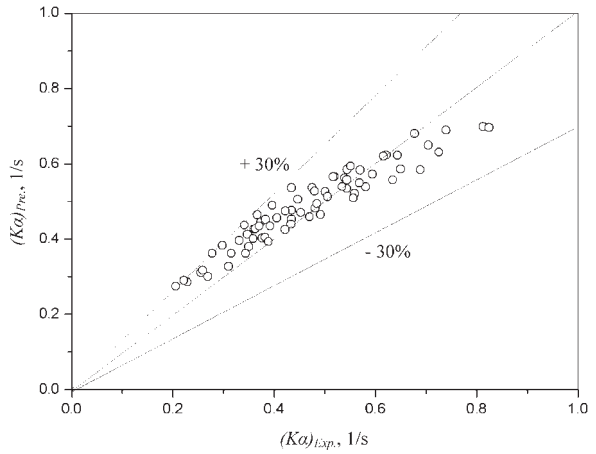

Figure 19. Comparison between experimental and predicted overall volumetric mass transfer coefficient.

minor dependence of Ka on U_{TP}. $(K\alpha)_{Exp}$ increased slightly with increasing U_{TP}. Though $(K\alpha)_{Pre.}$ is systematically larger than $(K\alpha)_{Exp.}$, $(K\alpha)_{Pre.}$ followed well the change trends of $(K\alpha)_{Exp.}$ Figure 18 showed that $K\alpha$ increased remarkably with increasing temperature. From Figures 12 and 18, effects of temperature on the conversion and overall volumetric mass transfer coefficient were similar.

In Figures 13–18, the predicted overall volumetric mass transfer coefficients were consistent with the experiment values, although noticeable deviation existed in a few cases. Based on the data given in Figures 13–18, Figure 19 further showed the experimental values versus predicted ones, and the error was within $\pm 30\%$.

Conclusions

With the hydrogenation of EAQ to EAHQ as a model reaction, effects of Taylor flow operating parameters on the reaction conversion and overall volumetric mass transfer coefficients were investigated in single square channel monolith reactors. Based on the present experiment and theoretical analysis, the following conclusions were drawn here:

(1) Under the present experiment conditions, a reasonable geometric model of Taylor bubble was developed in a square channel. Taylor flow patterns and hydrodynamic parameters were studied visually in transparent circular capillaries connected with reaction channels. The combination of the geometric model and visual study gained the real states of Taylor flow in opaque square reaction channels.

(2) EAQ conversion increased with increasing superficial gas velocity, gas bubble length and reaction temperature, while decreased with increasing superficial liquid velocity, liquid slug length and two-phase velocity. The hydrogenation of EAQ mainly proceeded on bubble wall regions, the contribution from slug wall regions to the reaction was minor. The ratio of gas bubble length to liquid slug length L_b/L_s, and gas bubble velocity V_b determined primarily EAQ conversion.

(3) Based on EAQ conversion, the experimental overall volumetric mass transfer coefficient, $(K\alpha)_{Exp.}$, was calculated. $(K\alpha)_{Exp.}$ was direct proportional to EAQ conversion per unit time. The experiment showed that $(K\alpha)_{Exp.}$ increased with increasing superficial gas velocity, gas bubble length, two-phase velocity and temperature, while decreased with enhancing superficial liquid velocity and liquid slug length.

(4) Four different mass transfer stages for hydrogen to catalyst wall were identified for Taylor flow in square channels. The film model, penetration model and Baten and Krishna's semi-empirial formulas[15] could be used to predict gas-solid, gas-liquid and liquid-solid volumetric mass transfer coeffecients, respectively. The predicted overall volumetric mass transfer coefficients followed well the change trend of experimental ones. As a whole, the errors were within $\pm 30\%$. For reactions restricted by mass transfer processes, the observed reaction rates could further be calculated by means of the predicted overall volumetric mass transfer coefficient.

Acknowledgments

The authors are grateful for the financial support for this work from National Natural Science Foundation of China (No. 20776138), Industry Project Foundation of Liaoning Province (No. 2007223021), and Innovation Fund of Dalian Institute of Chemical Physics, Chinese Academy of Sciences (No. K200602).

Notation

A_b = bubble cross-section area, m^2
A_c = square channel cross-section area, m^2
Ca = capillary number, $\mu U_{TP}/\sigma$
C_{EAQ}^{in} = EAQ concentration at reaction channel inlet, mol/m^3
C_{EAQ}^{out} = EAQ concentration at reaction channel outlet, mol/m^3
$C_{H_2}^{*}$ = hydrogen equilibrium concentration in EAQ solution, mol/m^3
$C_{H_2}^{wall}$ = hydrogen concentration on catalyst wall, mol/m^3
D = liquid phase diffusivity, m^2/s
d_c = channel hydraulic diameter, m
Gz_c = Graetz number based on reaction channel length $(L_c(1-\varepsilon_G)D/d_c^2V_b)$, dimensionless
Gz_s = Graetz number based on slug length $(L_sD/d_c^2V_b)$, dimensionless
K = mass transfer coefficient, m/s
$K\alpha$ = (overall) volumetric mass transfer coefficient, 1/s
L_b = gas bubble length, m
L_c = reaction channel length, m
r_{obs} = observed reaction rate, $mol/(m^3\ s)$
L_s = liquid slug length, m
Q_{film} = liquid volume flow rate around gas bubble, m^3/s
R_c = channel hydraulic radius, m
$R_{diag.}$ = bubble radius in diagonal direction, m
R_{side} = bubble radius in side direction, m
U_G = superficial gas velocity, m/s
U_L = superficial liquid velocity, m/s
U_s = liquid slug velocity, m/s
U_{TP} = two-phase superficial velocity, m/s
V_b = bubble velocity, m/s
X = EAQ conversion, dimensionless

Greek letters

α = specific interfacial area, 1/m
δ = liquid film thickness in side direction, m
ε_G = gas holdup, dimensionless
μ = kinetics viscosity, Kg/(m s)
σ = surface tension, N/m

Subscripts

b = Taylor bubble
c = reaction channel
cap = Taylor bubble cap
corner = the space between Taylor bubble arc surface and channel wall in Figure 6

Exp. = experimental values
film = liquid film between Taylor bubble flat surface and channel wall in Figure 6
G = gas phase
L = liquid phase
Pre. = predicted values
S = solid phase
s = liquid slug
UC = unit cell.

Literature Cited

1. Kreutzer MT, Kapteijn F, Moulijn JA, Heiszwolf JJ. Multiphase monolith reactor: chemical reaction engineering of segmented flow in microchannels. *Chem Eng Sci*. 2005;60:5895–5916.
2. Boger T, Heibel AK, Sorensen CM. Monolithic catalysts for the chemical industry. *Ind Eng Chem Res*. 2004;43:4602–4611.
3. Roy S, Bauer T, Al-Dahhan M, Lehner P, Turek T. Monoliths as multiphase reactors: a review. *ATCHE J*. 2004;50:2918–2938.
4. Cybulski A, Stankiewicz A, Edvinsson Albers RK, Moulijn JA. Monolithic reactors for fine chemical industries: a comparative analysis of a monolithic reactor and a mechanically agitated slurry reactor. *Chem Eng Sci*. 1999;54:2351–2358.
5. Kreutzer MT, Du P, Heiszwolf JJ, Kapteijn F, Moulijn JA. Mass transfer characteristics of three phase monolith reactors. *Chem Eng Sci* 2001;56:6015–6023.
6. Stankiewicz A. Process intensification in in-line monolithic reactor. *Chem Eng Sci*. 2001;56:359–364.
7. Tsoligkas AN, Simmons MJH, Wood J. Two phase gas-liquid reaction studies in a circular capillary. *Chem Eng Sci*. 2007;62:5397–5401.
8. Liu DS, Wang SD. Flow pattern and pressure drop of upward two-phase flow in vertical capillaries. *Ind Eng Chem Res*. 2008;47:243–255.
9. Liu DS, Wang SD. Hydrodynamics of Taylor flow in noncircular capillaries. *Chem Eng Process*. 2008;47:2098–2106.
10. Snyder LR, Adler HJ. Dispersion in segmented flow through glass tubing in continuous-flow analysis. *Anal Chem*. 1976;48:1017–1027.
11. Pedersen H, Horvath C. Axial dispersion in a segmented gas-liquid flow. *Ind Eng Chem Fundam*. 1981;20:181–186.
12. Trachsel F, Gunther A, Khan S, Jensen KF. Measurement of residence time distribution in microfluidic systems. *Chem Eng Sci*. 2005;60:5729–5737.
13. Bercic G, Pintar A. The role of gas bubbles and liquid slug lengths on mass transport in the Taylor flow through capillaries. *Chem Eng Sci*. 1997;52:3709–3719.
14. Baten JM, Krishna R. CFD simulations of mass transfer from Taylor bubbles rising in circular capillaries. *Chem Eng Sci*. 2004;59:2535–2545.
15. Baten JM, Krishna R. CFD simulations of wall mass transfer for Taylor flow in circular capillaries. *Chem Eng Sci*. 2005;60:1117–1126.
16. Vandu CO, Liu H, Krishna R. Mass transfer from Taylor bubbles rising in single capillaries. *Chem Eng Sci*. 2005;60:6430–6437.
17. Bercic G. Influence of operating conditions on the observed reaction rate in the single channel monolith reactor. *Catal Today*. 2001;69:147–152.
18. Natividad R, Kulkarni R, Nuithitikul K, Raymahasay S, Wood J, Winterbottom JM. Analysis of the performance of single capillary and multiple capillary (monolith) reactors for the multhphase Pd-catalyzed hydrogenation of 2-butyne-1,4-diol. *Chem Eng Sci*. 2004;59:5431–5438.
19. Tsoligkas AN, Simmons MJH, Wood J, Frost CG. Kinetic and selectivity studies of gas-liquid reaction under Taylor flow in circular capillary. *Catal Today*. 2007;128:36–46.
20. Mantle MD, Sederman AJ, Gladden LF, Raymahasay S, Winterbottom JM, Stitt EH. Dynamic MRI visualization of two-phase flow in a ceramic monolith. *AIChE J*. 2002;48:909–912.
21. Sederman AJ, Heras JJ, Mantle MD, Gladden LF. MRI strategies for characterizing two-phase flow in parallel channel ceramic monoliths. *Catal Today*. 2007;128:3–12.
22. Poling BE, Prausnitz JM, O'connell JP. *The Properties of Gases and Liquids*. New York: McGraw-Hill, Inc. 2001.
23. Qingdao College of Chemical Engineering. *Graph Handbook of Chemical Properties*. China: Chemical Industry Press, 2002.
24. Wei L. Ministructured catalyst bed for gas-liquid-solid multiphase catalytic reaction. *AIChE J*. 2002;48:1519–1532.
25. Kreutzer MT, Kapteijn F, Moulijn JA, Kleijn CR, Heiszwolf JJ. Inertial and interfacial effects on pressure drop of Taylor flow in capillaries. *AIChE J*. 2005;51:2428–2440.
26. Kolb WB, Cerro R. Coating the inside of a capillary of square cross section. *Chem Eng Sci*. 1991;46:2181–2195.
27. Thulasidas TC, Abraham MA, Cerro RL. Bubble-train flow in capillaries of circular and square cross section. *Chem Eng Sci*. 1995;50:183–199.
28. Sherwood TK, Pigford RL, Wilke CR. *Mass Transfer*. New York: McGraw-Hill, Inc., 1975.
29. Santacesaria K, Wilkinson P, Babini P, Carra S. Hydrogenation of 2-ethyltetrahydroanthraquinone in the presence of palladium catalyst. *Ind Eng Chem Res*. 1988;27:780–784.
30. Drelinkiewicz A, Kangas R, Laitinen R, Pukkinen A, Pursiainen J. Hydrogenation of 2-ethylanthraquinone on alumina-supported palladium catalysts: the effect of support modification with Na_2SiO_3. *Appl Catal A*. 2004;263:71–82.

Manuscript received May 30, 2008, and revision received Sept. 16, 2008.